NASA

Technical Memorandum 85035

AURORAL KILOMETRIC RADIATION/ AURORAL CORRELATION

Robert F. Benson and Syun-Ichi Akasofu

MAY 1983

National Aeronautics and Space Administration

Goddard Space Flight Center
Greenbelt, Maryland 20771

AURORAL KILOMETRIC RADIATION/AURORA CORRELATION

Robert F. Benson

Laboratory for Planetary Atmospheres

NASA/Goddard Space Flight Center

Greenbelt, MD 20771

Syun-Ichi Akasofu

Geophysical Institute of the University of Alaska

Fairbanks, Alaska 99701

May 1983

Presented at the National Radio Science Meeting in Boulder, Colorado (January 1983).

Accepted for publication in Radio Science (special issue on emissions from particle beams in space).

ABSTRACT

Auroral kilometric radiation (AKR) observations from the ISIS 1 topside sounder receiver were compared with visual auroral observations from the network of Alaskan all-sky camera stations. The goal was to relate AKR source region encounters to specific auroral forms on the same magnetic field line. Thirty eight simultaneous data sets were identified and analyzed. In general, intense AKR was associated with bright auroral arcs and conditions of weak or no AKR corresponded to times when either no aurora or only a faint arc or weak diffuse aurora were observed. Five cases, when both intense AKR and bright visual aurora were present, were analyzed in detail. Complete electron density N_e contours, from the satellite altitude down to the F region ionization peak, were obtained along N-S traversals of the AKR source region. In addition, the ISIS 1 orbital tracks were projected down the magnetic field-lines to the auroral altitude and compared to auroral features on a map derived from the all sky camera images. Density cavities (regions where $N_e < 100\ cm^{-3}$) were encountered on each of these passes. In one case the cavity extended in altitude down to just below 2000 km. The latitudinal extent of these cavities ranged from 3^o to almost 30^o. A variety of situations relating AKR to the visual aurora were identified and both spatial (within about 100 km at the satellite altitude), and temporal (within about 1 minute) correlations were identified. In addition to confirming that a density cavity is a necessary but not sufficient condition for the generation of AKR, the present results indicate that even the combination of a density cavity on an auroral-arc field line is not always sufficient for AKR generation. Thus, additional constraints must be satisfied in order to generate intense AKR from density cavities. These constraints most likely involve the characteristics of the energetic electron distribution function and possibly also latitudinal N_e gradients.

CONTENTS

INTRODUCTION

For nearly two decades the earth has been known to be an intense emitter of kilometer wavelength radiation. It has been correlated with high latitude magnetic disturbances [Dunkel et al., 1970] and with discrete auroral arcs [Gurnett, 1974]. Because of this latter correlation it has been called auroral kilometric radiation (AKR). It has also been shown to be an extremely sensitive indicator of magnetic substorms [Voots et al., 1977], to be directly related to the Frank and Ackerson [1971] inverted V type electron precipitation [Benson and Calvert, 1979; Green et al., 1979; Benson et al., 1980], field-aligned currents [Green et al., 1982], solar wind parameters [Gallagher and D'Angelo, 1981] and type III solar radio bursts [Calvert, 1981c].

The AKR/auroral correlation of Gurnett [1974] was based on observations of each phenomenon from distant satellites. Thus it represented an integrated correlation involving emissions and auroral forms over a large portion of the active auroral zone. The present correlative study obtains higher spatial and temporal resolution by employing a spacecraft (ISIS 1) which passes through the low altitude portion of the AKR source region together with the chain of Alaskan auroral all-sky camera stations. In this way, individual AKR source region encounters by the satellite could be compared with specific auroral forms on the same magnetic field line. Since AKR is so closely related to a number of geophysical parameters during periods of auroral activity, as outlined in the above paragraph, such a detailed correlation is likely to shed light on fundamental plasma processes taking place in the electric potential structure responsible for the acceleration of auroral particles (see the review by Akasofu [1981] and related papers in the AGU monograph based on the Chapman Conference on "The Formation of Auroral Arcs").

OBSERVATIONS

The main task of the present investigation is to compare two data sets - each capable of remote observations. One is based on the photographic recording of the aurora over Alaska using a network of all-sky cameras. Each of these cameras monitors the aurora over approximately 10^{o} latitude every 30 seconds or one minute (depending on station) with a 15 sec exposure on tri-x film and is capable of resolving stable features of the order of 10 km near the center of the all-sky camera image. The other data set is based on the detection of AKR with the ISIS 1 topside sounder receiver. During nighttime apogee passes over the auroral zone, ISIS 1 frequently encounters the low altitude portion of the AKR source region as was first demonstrated by Benson and Calvert [1979]. In general, ISIS 1 samples the AKR once every 30 sec giving a spatial resolution of around 200 km. This temporal and spatial resolution is increased during certain operating modes. Even when the satellite does not encounter an AKR source, the sounder receiver can often detect intense radiation over distances $\sim 10^{3}$ km.

The present investigation was initiated by considering 164 ISIS 1 high altitude nighttime passes over Alaska. Of these, 38 corresponded to conditions of fairly clear sky with all-sky camera data available from one or more of the stations of the all-sky camera network with ISIS 1 at least 15^{o} above the horizon. ISIS 1 takes about one minute to cross the field-of-view of a given all-sky camera under the near-apogee conditions considered here.

The 38 correlative events are summarized in Table 1. The times, under the column heading "mid-point UT", in general correspond to the mid-point of the satellite pass over the primary station of interest. The observed ISIS 1 AKR intensity levels, on a Ø to 3 scale, are classified into the next 7 columns. The first 6 of these correspond to auroras whereas the last one

corresponds to conditions of weak or no aurora. Among the first 6 columns, the intensity of auroral activity is ordered from most active (left) to least active (right). The comment "hazy (no arc)", pertaining to entries in the "weak or no aurora" column, means that the sky conditions could have masked a faint diffuse aurora but a discrete arc would have been detected if present. The most striking feature in this table is that the intense AKR events (intensity level 3) are clustered in the first 2 columns corresponding to active and/or bright auroral arcs, whereas satellite/ground-station comparisons corresponding to conditions with weak or no AKR (1 or 0 intensity scale) are clustered in the last column corresponding to conditions of weak or no aurora.

An example of intense AKR, i.e., a 3 in Table 1, as observed by ISIS 1 is given in Figure 1. A reproduction of the actual data is given in the lower panel and a schematic illustration in the top panel. The schematic is used to help clarify which features are due to the reception of ionospheric echoes resulting from the stimulating sounder pulse and which are due to natural signals such as AKR. Two types of echoes are received: those due to the reflection of electromagnetic waves (traveling at approximately the velocity of light) from the denser ionosphere hundreds to thousands of kilometers below the satellite and echoes of electrostatic waves (traveling at approximately acoustic velocities) reflected within hundreds to thousands of meters from the satellite. The latter reflections occur because of the sensitivity of the dispersion relations, near resonant conditions, to small changes in the ambient magnetic field $\vec{B}$ and/or the electron density N_e. The electromagnetic reflections are used in inversion techniques to derive N_e profiles from the satellite altitude down to the altitude of the F layer ionization peak [see, e.g., Jackson, 1969]. The electrostatic reflections are used to determine in-

situ values for the electron gyrofrequency f_H and the plasma frequency f_N [see, e.g., Benson, 1977]. These reflections are received at a variety of delay times immediately after the termination of the 0.1 msec sounder pulse. Because of the wide receiver bandwidth (50 kHz) they appear as stalactites hanging down from the zero-baseline and have been described as "resonances". These resonances seldom extend the full 30 msec of delay time on the ionogram display. The signals due to AKR, on the other hand, are not synchronized to the sounder pulse and are observed over the entire receiver listening time between pulses. The resonant features, especially at f_H are often masked by intense AKR (as in Figure 1). In such cases, f_H is determined from the observed nf_H resonances with $n > 1$. In addition, a consecutive sequence of ionograms often must be investigated to identify particular features with confidence.

Such a sequence of consecutive ionograms is presented in Figure 2. The ionogram of Figure 1 corresponds to a portion of ionogram d of Figure 2. On the original film, fundamental AKR near 0.5 MHz can be detected on each of the 8 ionograms of Figure 2. (Note, since there is some loss involved in each step of photographic reproduction, some of the features discussed may not be apparent. The reproduction in Figure 2 is a negative made directly from the positive film available at the National Space Science Data Center at Goddard; thus the AKR signals appear here as white noise-bands covering the entire ionogram virtual range scale. All other ionogram reproductions used in this paper involved one more photographic step to obtain positive prints.) Similarly, 2nd harmonic AKR near 1.0 MHz on the swept-frequency portion of the ionograms (right side) can be detected on the original film on all ionograms but the one labeled h, 3rd harmonic AKR on b (trace), c & d, and a trace of 4th harmonic AKR on d. These harmonics are considered to be due to the AKR

rather than to instrumental nonlinearities [Benson, 1982].

The long time-duration fixed-frequency portions of the ionograms of Figure 2 (the left 3/4 of each ionogram) provide high time-resolution information on the AKR 2nd harmonic. During this sequence, f_H continuously decreased from 0.513 MHz (a) to 0.428 MHz (h). The direction of this frequency change can be seen in Figure 2 by noting that the sounder-stimulated electrostatic plasma wave resonance at $2f_H$ (labeled 2H) appears slightly above the 1.0 MHz frequency marker in the swept-frequency portion of ionogram a but is well below it in ionogram h. As $2f_H$ passes through 1.0 MHz this short time-duration stimulated $2f_H$ resonance is detected within the bandwidth of the receiver during periods of fixed frequency sounder operation (at 1.0 MH_z). This signal, while observed on part of a and c, is most apparent on b as the dark wavy pattern on the top of the fixed-frequency portion of the ionogram. When $2f_H$ is sufficiently below 1.0 MHz, the 2nd harmonic AKR signal falls within the bandwidth of the receiver during the periods of fixed frequency sounder operation. This condition is first satisfied about midway through the fixed-frequency portion of ionogram c. Unlike the $2f_H$ stimulated resonance (which is fading out on the fixed-frequency record as the AKR is building up) the AKR is not synchronized with the zero time base and is observed over the entire listening interval. This 2nd harmonic AKR is strongest on d and e and traces of it can be observed on the following ionograms of Figure 2. The signal nulls caused by the rotating dipole antenna pattern are clearly evident on d (see also Figure 1). James [1980] has used such null patterns to determine AKR direction of arrival information.

ISIS 1 was in the AKR source region during the recording of ionograms d and e of Figure 2. Identification of such source encounters are based on the closing of the frequency gap between the f_H resonance and the fundamental AKR

[Benson and Calvert, 1979]. In the present investigation, such source encounters were based on the closing of the frequency gap between the $2f_H$ resonance and the 2nd harmonic AKR band. This procedure increases the accuracy of the technique so that a "zero-gap" condition on the fundamental can be determined to about 13 kHz rather than 25 kHz (1/2 of the receiver bandwidth). The resulting source determination is then within $\gtrsim$ 100 km [Calvert, 1981a]. The 2nd harmonic was chosen, rather than a higher harmonic because it is observed much more often.

Figure 3 shows the ISIS 1 orbital track (projected along $\vec{B}$ to 100 km altitude) corresponding to the data of Figure 2 on an Alaskan map with superimposed auroral features, N_e contours from the satellite altitude down to the F peak and representative all-sky camera auroral images. On this night there was no major change in the auroral activity during the passage of the satellite. The changes were mainly in the growth and decay of individual arcs within a multiple arc system. As can be seen in the map at the upper left of Figure 3, the field lines corresponding to this auroral arc system were encountered between the recording of ionograms c and d. The auroral image at the lower left corresponds approximately to the time of the start of the fixed-frequency portion of ionogram c of Figure 2; the image at the lower right to a time near the end of the fixed-frequency portion of ionogram d of Figure 2. The AKR source encounters on d and e appear slightly equatorward of the field lines threading the main arc system as indicated on the Alaskan map and also (in cross section) at the 100 km level of the N_e contour diagram in Figure 3. One of the most outstanding features of this contour diagram is the great extent of the N_e cavity (i.e., the region where $N_e < 100$ cm^{-3}) both in latitude (27^o) and in altitude (down to 1800 km). In this contour diagram the AKR source region encounters are identified by magnetic field lines projected

through the satellite positions; the heavier portions of these lines correspond to the altitude region of AKR generation. These regions are determined by assuming that the maximum frequency observed in the fundamental AKR band on ionograms near the source field-line encounter correspond to emissions originating near the extraordinary (x) mode cutoff frequency f_x at lower altitudes [Benson and Calvert, 1979].

The AKR recorded during the fixed frequency portions of ionograms d and e does not show any intensity modulation corresponding to satellite motion in and out of field lines associated with individual arcs. This lack of modulation is probably due to the reception of propagating AKR and to the close spacing of the arcs ($\lesssim$ 100 km) relative to the resolution of AKR source encounters ($\gtrsim$ 100 km) at the satellite altitude.

The AKR intensity key in Figure 3 (upper right) is based on the following convention: weak - just detectable on ionogram film, moderate - very definite signal but AGC voltage does not saturate, strong - AGC voltage saturates but intensity modulation still detected on video signal, intense - AGC voltage and video signal both saturate, i.e., the signal display on the ionogram is solid black. All of these classifications are present in the a-h sequence in the N_e contour diagram of Figure 3; they can be compared with the corresponding fundamental AKR signals on the ionograms of Figure 2.

Figure 4 shows AKR, N_e and auroral information corresponding to conditions of a fairly bright arc which showed no major change during the passage of the satellite. The first AKR source encounter (on ionogram c) corresponds to a position in the diffuse glow equatorward of the auroral arc as illustrated on the map at the top left of Figure 4. The fixed-frequency portion of ionogram c reproduced at the bottom of Figure 4 indicates that intense 2nd harmonic AKR was detected midway between the b and c points on the satellite

track, i.e., closer to the arc location. Again, spin modulation is observed during the fixed-frequency operation which, in this case, corresponds to the high frequency side of the 2nd harmonic AKR (as can be seen from the position of this AKR band relative to the 1.0 MHz frequency marker on the swept-frequency portion of ionogram c). Thus this signal corresponds to emissions originating below the satellite, i.e., regions of higher $2f_H$.

Figure 5 shows similar data for a more active auroral event. It began with the brightening of an auroral arc on the northwest horizon of Inuvik at 0951 UT. By 0954 it stretched across the northern sky and after 0956 it developed a wavy structure and increased considerably in brightness. It developed into a fast traveling form resembling an inverted Ω, the so-called Ω band [Akasofu and Kimball, 1964] which was gone from the field of view of the Inuvik camera by 1005. The Ω band shape at 0958 (the time corresponding to the satellite position just shy of the midway point between ionograms b and c) is shown on the map in Figure 5. Ionogram b marks a sudden transition from weak to intense AKR. It does not correspond to an AKR source region encounter, but the gap between the $2f_H$ resonance and the 2nd harmonic AKR band is smaller than on the following ionograms (e.g., compare the b and c ionograms on the right side of Figure 5). Thus the satellite was closest to the AKR source, during the reception of intense AKR, when ionogram b was recorded. The widening of the frequency gap on later, more equatorward, ionograms indicates motion away from the source. These observations are consistent with an AKR source on the field lines associated with the active arc to the north (see map in Figure 5). Also consistent with this source location is the increase in AKR intensity from weak to moderate and then back to weak as ISIS 1 crossed the field lines associated with the location of the still quiet arc at 0956 UT (this time corresponds to the midpoint between the

two open triangles, designating moderate AKR, near 66° latitude on the N_e contour diagram in Figure 5). This position was not noted as an AKR source region encounter because there appeared to be a mixture of ordinary (o) and extraordinary mode AKR (the distinction between o and x-mode AKR on ISIS 1 ionograms is the subject of a companion paper [Benson, 1983]) and the 2nd harmonic AKR was observed at a frequency less than the stimulated $2f_H$ resonance indicating that these signals originated from a source above the satellite. Thus, even though moderate fundamental AKR was observed just above f_H (indicating a source below the satellite), the source region criterion for this paper - zero gap between the 2nd harmonic AKR and the $2f_H$ stimulated resonance - was not satisfied.

The fundamental AKR signal extends to considerably higher frequency on ionogram c than on b in Figure 5. On the original film it is apparent that most of this high frequency broadening is due to a distinctly separate frequency band. The separation between these frequency components may be visible on the reproduction in Figure 5 as a slight dip in the white AGC trace against the black AKR band at 0.58 MHz on ionogram c. An example with a more distinct frequency separation is shown in Figure 5 of Benson [1982]. Such AKR frequency components are suggestive of two distinct frequency sources. The double hump structure of the auroral Ω band (see map in Figure 5) may be the visual manifestation at auroral altitudes of such a double AKR source at higher altitudes. Frequency components are sometimes identified in the vicinity of extremely sharp latitudinal N_e gradients. For example, the last ionogram with intense AKR, which was observed at such a gradient (see the solid triangle near 56° latitude on the N_e contour plot of Figure 5), also revealed AKR components on the fundamental. Some interference was observed equatorward of this N_e boundary, along with what appeared to be o-mode AKR.

Figure 6 shows N_e contours (with AKR information) and an Alaskan map (with auroral information) for a case of a fairly bright stable arc which existed outside of a field-line projected N_e cavity. Unlike the cases of Figures 3, 4 and 5 this cavity (i.e., the region where $N_e < 100$ cm^{-3}) is restricted to only about 3^o in latitude. Strong x-mode AKR source region encounters were only observed within this cavity (see b and c on the contour diagram in Figure 6) even though no auroral forms were associated with field lines through this region. On both of these ionograms (as well as the preceding 2 and the following one) the 2nd harmonic AKR was stronger than the fundamental. Ionogram c was presented as Figure 7 of Benson [1982]. The intense AKR observed just equatorward of the N_e cavity (i.e., the solid triangle near 53^o latitude) corresponds to o-mode radiation based on identification arguments given in the companion paper by Benson [1983]. Ionogram a indicated an x-mode AKR source region encounter of moderate intensity. This ionogram also revealed the presence of o-mode AKR. The ionogram prior to ionogram a could be considered as a source region encounter with the lower boundary of the source at the satellite altitude since the zero frequency gap in this case was between the high frequency edge of the 2nd harmonic AKR signal and the $2f_H$ resonance; this ionogram, which also revealed fundamental o mode AKR, was presented as Figure 10 of Benson [1982]. Note the continuity of the lower edge of the AKR density cavity extending through the satellite position in this case (corresponding to the open triangle to the right of a) and the lower boundary cross bars on the field lines through a, b and c. Ionogram d corresponded to an o-mode AKR source region encounter when $f_N/f_H = 1.0$ is reproduced in the companion paper (see the top ionogram of Figure 4 of Benson [1983]). The two horizontal bars on the field-line going through this ionogram represent the uncertainty in this case in the determination of the

lower edge of the source region. The uncertainty arises from variations in the upper frequency edge of the fundamental AKR band; the projection in this case (of o-mode AKR) is based on f_{ll} rather then f_x.

The time corresponding to the satellite crossing of the arc field-line (1350:30) corresponds approximately to the 3rd satellite position from the right (i.e., near 63^0 latitude) on the contour diagram of Figure 6. No increase in AKR signal intensity was observed in this vicinity which was outside the N_e cavity. Recall that in the case of Figure 5 an increase in AKR intensity was observed at such a crossing when the (still quiet) arc was associated with an N_e cavity at higher altitudes.

Figure 7 presents results from an intermediate case from the N_e contour point-of-view, i.e., an extended N_e cavity is bifurcated by a high density region centered at about 61^0 latitude. The aurora was very active. At 0710 UT, prior to the satellite passage, a very bright arc was in the northern sky of College. A fairly intense westward traveling surge appeared near the eastern end of the arc, indicating the onset of a fairly intense substorm in the midnight sector (over central Canada). The arc was displaced northward as the surge propagated along the arc. By 0720 UT, as the satellite approached Alaska from the north, the surge was near the western horizon and the College sky was filled with arc segments which were mostly N-S aligned. This condition lasted until about 0740 UT. During the passage of ISIS 1, the general condition was similar, although the auroral forms were in a turbulent condition. The arcs for 0723 and 0724 UT are shown on the map in Figure 7.

With only one exception, the AKR detected by ISIS 1 was only weak to moderate during this period of great auroral activity. The exception is found in one ionogram corresponding to an x-mode AKR source region encounter at the steep N_e gradient near 59^0 latitude (ionogram b in Figure 7). On the adjacent

ionogram (a) a moderate intensity AKR source was encountered. This AKR, which appeared to also have an o-mode component, corresponded to a local N_e peak. Both ionograms a and b were recorded when the satellite was very close to auroral arc field lines (see Figure 7). Only weak AKR, on the other hand, was observed as the satellite crossed the field-line of the bright arc in the north near 70^o latitude which was associated with the traveling westward surge earlier (the relevant satellite position on the N_e contour diagram is the 4th open circle from the right). There was no noticeable AKR enhancement even though ISIS 1 was within an N_e cavity, i.e., $N_e < 100$ cm^{-3}, as it crossed the arc field line.

DISCUSSION

The general results given in Table 1 indicate a very good correlation between AKR and the aurora. The exceptions involve cases of AKR signatures corresponding to a remote source (see remarks under "comments" column in the table) and are probably due to propagation effects. While the overall comparisons (which compares maximum intensity AKR with maximum auroral activity during a satellite pass) is impressive, a detailed look at 5 cases reveal the importance of (1) the N_e cavity, (2) propagation effects, (3) temporal and spatial correlations, and (4) N_e gradients.

Density cavity. The observations that AKR originates within N_e depletions [Benson and Calvert, 1979; Benson et al. 1980; Calvert, 1981b] is fundamental to AKR theories predicting x-mode radiation with a frequency near f_H [Melrose, 1976; Wu and Lee, 1979; Grabbe et al., 1980]. In most of the 5 cases examined here in detail, the latitudinal extent of the density cavity ($N_e < 100$ cm^{-3}) was far greater than that of either the auroral arcs or the AKR source region. This finding, relative to AKR, is consistent with the

results based on an additional 9 ISIS 1 passes (see Figure 12 of Benson [1981]). It is possible to detect intense AKR far removed from the source region when the cavity is large (as in Figures 3, 4 and 5) but not when it is small (see Figures 6 and 7).

Propagation effects. The observations that AKR is in the x mode and propagates nearly perpendicular to $\vec{B}$ [Benson and Calvert, 1979] is fundamental to the theories of Melrose [1976], Wu and Lee [1979] and Grabbe et al. [1980]. The present observations reinforce the earlier observations and emphasize the importance of propagation effects in the detection of AKR. For example, the continuity of auroral observations during the event of Figure 3 indicates that the lack of significant AKR detection poleward of 67^{o} latitude was not likely a temporal effect. The field line geometry, initial propagation nearly perpendicular to $\vec{B}$ and upward refraction due to $\nabla\vec{B}$ [Benson and Calvert, 1979; Calvert, 1981a] are very consistent with the AKR observations of Figure 3. Similar arguments hold for the event of Figure 4. In this case, however, the higher satellite altitude allowed AKR to be detected over greater distances. As the satellite approaches the source region the AKR intensity increases from moderate to strong to intense well before the source field-line is encountered.

In Figure 5 the satellite altitude was also high but in this case temporal effects (deduced from the auroral observations) appear to limit the observations of intense AKR prior to the time when ionogram b was recorded. Once the source became active (believed to be located between the open triangles near 66^{o} in Figure 5 - again based on the auroral observations) intense AKR, with a signature of a remote source, was received until the satellite crossed the sharp N_e boundary near 55^{o} latitude. Again, the tilt of $\vec{B}$, initial propagation direction, upward refraction and high satellite

altitude would favor AKR reception within the N_e cavity.

AKR/aurora temporal and spatial correlations. The present results support the observations of Gurnett [1974] that active aurora and intense AKR are correlated. This support comes from the general comparisons of Table 1 and the more detailed comparisons which reveal dramatic spatial correlations (see Figures 3, 4 and 7) and the temporal comparison of Figure 5. There is some indication that the AKR source region extends equatorward of the auroral field-lines (see Figures 3 and 4).

It is found, however, that a spacecraft encounter with a field-line through a bright arc is not always sufficient for AKR generation (see Figure 6 and the arc near 70^{o} in Figure 7). Even an active arc within an N_e cavity is not always sufficient (see the above Figure 7 example). Thus, additional constraints - most likely on the pertinent energetic electron distribution function must be satisfied to stimulate AKR. Such constraints, based on direct particle/AKR source region correlations, have been reported by Benson et al. [1980]. The importance of the energetic distribution function characteristics has been recently emphasized by Melrose et al. [1982], Omidi and Gurnett [1982], Wu et al. [1982], Dusenbery and Lyons [1982], Hewitt et al. [1982] and Hewitt and Melrose [1983].

It is also found that an AKR source can be located in a region where there is no auroral activity (Figure 6). This particular event was notable in that the AKR 2nd harmonic was considerably more intense than the AKR fundamental in the source region and most of the AKR outside of the source region was dominated by o-mode radiation. This o-mode dominance was particularly evident in the higher density region on the low latitude side of the N_e cavity [Benson, 1983].

Electron density gradients. Another notable feature of the above event, i.e., the one corresponding to Figure 6, is the extremely sharp latitudinal N_e gradient near 53^o latitude. It may be more than a coincidence that such steep gradients are associated with strong 2nd harmonic AKR (relative to the fundamental) in this case. The harmonic AKR may be due to a nonlinear response of the inhomogeneous medium to the fundamental AKR. Alternatively, it may due to the reception of signals from sources in the nearby denser plasma as discussed two paragraphs below.

Another example of a possible effect of N_e gradients on the observed AKR spectrum is given in the event of Figure 5. As mentioned earlier, frequency components were observed on the fundamental AKR on the ionogram corresponding to the satellite position just inside the density cavity boundary at 55^o latitude.

The greatest effect, however, appears to be in the restrictive effects on AKR caused by small N_e cavities such as existed in the events of Figures 6 and 7 (considering the AKR cavity in Figure 7 to be the small one between 55 and 60^o latitude where intense AKR is observed). Two possible causes for this restriction of AKR are suggested: a limitation of the required instability growth region (e.g., see Wu and Lee [1979]) or propagation restrictions due to refractive effects. These propagation restrictions would be less severe for the 2nd harmonic AKR mentioned above than for the fundamental AKR because the former experiences less refraction since it is well displaced in frequency from the x-mode cutoff at f_x. Thus the relatively strong 2nd harmonic AKR (relative to the fundamental) may be due to the reception of signals from a number of sources located in nearby regions of higher plasma density - where theory predicts stronger 2nd harmonic x-mode AKR than fundamental x-mode AKR e.g., see Lee et al. [1980] and Melrose et al. [1982].

Information pertaining to such effects is limited to only the N-S direction if only the ISIS 1 observations are considered. Longitudinal E-W information can be inferred from the auroral observations. Thus it may be reasonable to assume that the enhanced N_e structure near the satellite altitude between 65 and 70° in the bottom left of Figure 5 could extend along the direction of the arc displayed near 70° (at 100 km altitude) in the map in upper left part of Figure 5. The growth and propagation of AKR in the E-W direction could then account for the slight AKR enhancement observed during the crossing of the arc field line by ISIS 1.

SUMMARY

Intense AKR is highly correlated with bright aurora. Electron density cavities above about 2000 km altitude, which are required for the generation of intense AKR, can have a far greater latitudinal extent than either the region of auroral-arc field-lines or the AKR source region. While there is a good overall AKR/Aurora correlation, an auroral-arc field-line within an N_e cavity does not always lead to AKR and it is possible to generate AKR within a cavity even when there is no auroral activity on the associated magnetic field line. The concept of an initial propagation angle nearly perpendicular to $\vec{B}$, with subsequent upward refraction of the waves, is supported by the pattern of observed AKR intensity far outside the source region. Such AKR, i.e., detected far from the source, is not observed to be intense when the N_e cavity is limited to a small latitudinal region. Strong latitudinal N_e gradients appear to play an important role in the generation of specific AKR features such as harmonics, frequency components and wave polarization.

Acknowledgements. We are grateful to M. Posey for assistance in the data analysis. Photographic reproductions of the ISIS 1 ionograms were made by the National Space Science Data Center at the Goddard Space Flight Center. J. Jackson kindly provided comments on the manuscript. Part of this work was supported by a NASA grant (NSG-7447) and a NSF grant (ATM-81-15321) to the University of Alaska.

REFERENCES

Akasofu, S.-I., Auroral arcs and auroral potential structure, in Physics of Auroral Arc Formation, Geophysical Monograph 25, pp. 1-14, American Geophysical Union, Washington, D.C. 1981.

Akasofu, S.-I., and D. S. Kimball, The dynamics of the aurora - I Instabilities of the aurora, J. Atmos. Terr. Phys., 26, 205-211, 1964.

Benson, R. F., Stimulated plasma waves in the ionosphere, Radio Sci., 12, 861-878, 1977.

Benson, R. F., Auroral kilometric radiation source region observations from ISIS 1, in Physics of Auroral Arc Formation, Geophysical Monograph 25, pp. 369-379, American Geophysical Union, Washington, D.C., 1981.

Benson, R. F., Harmonic auroral kilometric radiation of natural origin, Geophys. Res. Lett., 9, 1120-1123, 1982.

Benson, R. F., Ordinary mode auroral kilometric radiation - with harmonics - observed by ISIS 1, Radio Sci., in press, 1983, also NASA Technical Memorandum 85036, Goddard Space Flight Center, Greenbelt, MD 20771, May, 1983.

Benson, R. F., and W. Calvert, ISIS 1 observations at the source of auroral kilometric radiation, Geophys. Res. Lett., 6, 479-482, 1979.

Benson, R. F., W. Calvert, and D. M. Klumpar, Simultaneous wave and particle observations in the auroral kilometric radiation source region, Geophys. Res. Lett., 7, 959-962, 1980.

Calvert, W., The signature of auroral kilometric radiation on ISIS 1 ionograms, J. Geophys. Res., 86, 76-82, 1981a.

Calvert, W., The auroral plasma cavity, Geophys. Res. Lett., 8, 919-921, 1981b.

Calvert, W., The stimulation of auroral kilometric radiation by type III solar radio bursts, Geophys. Res. Lett., 8, 1091-1094, 1981c.

Dunckel, N., B. Ficklin, L. Rorden, and R. A. Helliwell, Low-frequency noise observed in the distant magnetosphere with OGO 1, J. Geophys. Res., 75, 1854-1862, 1970.

Dusenbery, P. B. and L. R. Lyons, General concepts on the generation of auroral kilometric radiation, J. Geophys. Res., 87, 7467-7481, 1982.

Frank, L. A., and K. L. Ackerson, Observations of Charged particle precipitation into the auroral zone, J. Geophys. Res., 76, 3612-3643, 1971.

Franklin, C. A., and M. A. Maclean, The design of swept-frequency topside sounders, Proc. IEEE, 57, 897-929, 1969.

Gallagher, D. L. and N. D'Angelo, Correlations between solar wind parameters and auroral kilometric radiation intensity, Geophys. Res. Lett., 8, 1087-1089, 1981.

Grabbe, C. L., K. Papadopoulos, and P. J. Palmadesso, A coherent nonlinear theory of auroral kilometric radiation 1. Steady state model, J. Geophys. Res., 85, 3337-3346, 1980.

Green, J. L., D. A. Gurnett, and R. A. Hoffman, A correlation between auroral kilometric radiation and inverted V electron precipitation, J. Geophys. Res., 84, 5216-5222, 1979.

Green, J. L., N. A. Saflekos, D. A. Gurnett and T. A. Potemra, A correlation between auroral kilometric radiation and field-aligned currents, J. Geophys. Res., 87, 10463-10467, 1982.

Gurnett, D. A., The earth as a radio source: terrestrial kilometric radiation, J. Geophys. Res., 79, 4227-4238, 1974.

Hewitt, R. G., and D. B. Melrose, Electron cyclotron maser emission near the cutoff frequencies, Aust. J. Phys., in press, 1983.

Hewitt, R. G., D. B. Melrose, and K. G. Ronnmark, The loss-cone driven electron-cyclotron maser, Aust. J. Phys., 35, 447-471, 1982.

Jackson, J. E., The reduction of topside ionograms to electron-density profiles, Proc. IEEE, 57, 960-976, 1969.

James, H. G., Direction-of-arrival measurements of auroral kilometric radiation and associated ELF data from ISIS 1, J. Geophys. Res., 85, 3367-3375, 1980.

Lee, L. C., J. R. Kan, and C. S. Wu, Generation of auroral kilometric radiation and the structure of auroral acceleration region, Planet. Space Sci., 28, 703-711, 1980.

Melrose, D. B., An interpretation of Jupiter's decametric radiation and the terrestrial kilometric radiation as direct amplified gyroemission, Astrophys. J., 207, 651-662, 1976.

Melrose, D. B., K. G. Ronnmark, and R. G. Hewitt, Terrestrial kilometric radiation: the cyclotron theory, J. Geophys. Res., 87, 5140-5150, 1982.

Omidi, N. and D. A. Gurnett, Growth rate calculations of auroral kilometric radiation using the relativistic resonance condition, J. Geophys. Res., 87, 2377-2383, 1982.

Voots, G. R., D. A. Gurnett, and S.-I. Akasofu, Auroral kilometric radiation as an indicator of auroral magnetic disturbances, J. Geophys. Res., 82, 2259-2266, 1977.

Wu, C. S. and L. C. Lee, A theory of the terrestrial kilometric radiation, Astrophys. J., 230, 621-626, 1979.

Wu, C. S., H. K. Wong, D. J. Gorney and L. C. Lee, Generation of the auroral kilometric radiation, J. Geophys. Res., 87, 4476-4488, 1982.

Table 1. AKR/Aurora Comparisons. AKR intensity (classified by auroral type): Ø None, 1 Weak, 2 Moderate, 3 Intense

Yr	Date Mo	Date Day	Mid-point UT	Active Arcs	Bright Arc	Bright Diffuse	Weak Diffuse	Faint Arc	Weak Glow	Weak or no Aurora	Comments
69	10	31	1352		3						See Figure 6
	11	10	1125	3							Extremely intense substorm
	12	1	1026		3						Hazy
	12	2	0957	3							See Figure 5
	12	7	0950						1		Weak substorm 1/2 hr earlier
	12	13	0913	3							
	12	22	0924		1						AKR remote; arc on horizon
70	10	19	1113							1	No aurora, bright moon
	10	24	0850							Ø	Hazy (no arc)
	10	25	1035							Ø	Hazy (no arc), poor all-sky camera film
	11	6	0919				1				
	12	4	0707		3						
	12	5	0637		3						See Figure 4
	12	6	0604							3	AKR remote; no aurora
	12	8	0724	3							See Figure 7
	12	9	0657							3	AKR remote; hazy (no arc), moon
	12	27	0457					Ø			
	12	31	0517							Ø	No aurora but may be overcast
71	10	24	0731							1	AKR remote; hazy (no arc)
	10	28	0746		3						AKR remote; arc on horizon, diffuse near zenith
	10	29	0721	3							See Figure 3
	11	9	0630					1			AKR remote; faint arc in N. Sky
	11	10	0602		3						AKR remote; bright arc on horizon
	11	14	0621					1			AKR remote, arc on horizon
	11	20	0543		2						AKR remote; arc (medium intensity) near horizon
	11	25	0532		3						AKR local & remote; arc near horizon
	12	6	0443							Ø	Possible glow near horizon
	12	12	0402						Ø		Glow near horizon
	12	19	0253							1	AKR remote; no aurora but fairly bright twilight
	12	23	0311							Ø	No aurora
72	10	13	0543							Ø	No aurora
	11	4	0402							Ø	No aurora
	11	15	0311							Ø	No aurora
	11	25	0247							Ø	No aurora
	11	26	0219		2						Bright arc seen in twilight
	12	1	0209							Ø	No aurora
	12	18	0035							Ø	No aurora but bright moon
73	11	29	1232			3					

Figure Captions

Figure 1. ISIS 1 ionogram (bottom) and schematic illustration (top) corresponding to an AKR source region encounter. The electrostatic (es) ionospheric echoes (or sounder-stimulated plasma resonances) designated by N, H and nH correspond to f_N, f_H and nf_H, respectively. The electron density is so low that f_N is well below the lower limit (0.1 MHz) of the swept-frequency portion of the ionogram and the cutoff frequency f_x of the electromagnetic (em) x-mode ionospheric echo merges with f_H (within the 50 kHz receiver bandwidth). The flat top of the automatic gain control (AGC) voltage corresponds to the saturation level for this signal which is reached well before the ionogram video signal saturates. For further instrumental details see Franklin and Maclean [1969]. The ionogram was recorded on 29 October 1971 0721:36 UT (corresponding to H on the swept-frequency portion) 2018 magnetic local time MLT, 3142 km altitude, 65.8° invariant latitude Λ when $f_N/f_H < 0.11$.

Figure 2. ISIS 1 AKR observations over Alaska on 29 October 1971 from 0718:43 (f_H time on ionogram a) to 0725:27 UT (f_H time on ionogram h). In this case the delay time scale is marked by the conventional method of echo virtual range, i.e., assuming the light speed c for the electromagnetic waves stimulated by the sounder pulse. A portion of ionogram d of this sequence was used in Figure 1.

Figure 3. Fort Yukon auroral observations during the ISIS 1 AKR observations of Figure 1 and 2 on 29 October 1971. Also shown are N_e contours from the satellite position down to the F layer peak density. They

were determined from vertical N_e profiles deduced from the em ionospheric reflection traces on each ionogram. The satellite position at the time of each ionogram is indicated by an asterisk if no AKR was observed or by a symbol (see key) indicating the observed AKR intensity. An AKR source region encounter is identified by a magnetic field line projected through the satellite position. The heavy portion of this field line indicates the extent of the AKR source region below the satellite. The contours represent a vertical cross-section along the orbital track shown on the map. This track represents a field-line projection of the ISIS 1 orbit down to an assumed aurora altitude of 100 km. The arcs corresponding to the all sky camera image in the lower right, which in turn corresponds to the time of recording ionogram d (from Figures 1 and 2), are drawn on this map. The dashed line represents an arc that was significantly fainter than the others. The intersection points between these arcs and the projected satellite track are shown as dots at the 100 km level of the N_e contour diagram. The small dots across the map of Alaska represent all-sky camera stations. The relevant station for the present observations, Fort Yukon, is circled and marks the end of an arrow designating geomagnetic north. The field-line-projected subsatellite track (down to 100 km) is also shown as a curved dashed line on each auroral image; the open circle designates the projected satellite position at the indicated time.

Figure 4. Inuvik auroral observations and ISIS 1 AKR and N_e observations on 5 December 1970 0637:32 UT (ionogram b), 2000 MLT, 3305 KM, 70.3° Λ, $f_N/f_H \leq 0.11$.

Figure 5. Inuvik auroral observations and ISIS 1 AKR and N_e observations on 2 December 1969 0957:40 UT (ionogram b), 2306 MLT, 3452 km, 68.4° Λ, $f_N/f_H \leq 0.11$.

Figure 6. Kotzebue auroral observations and ISIS 1 AKR and N_e observations on 31 October 1969 1359:29 UT (b), 0136 MLT, 3019 km, 60.6° Λ, $f_N/f_H = 0.17$.

Figure 7. College auroral observations and ISIS 1 AKR and N_e observations on 8 December 1970 0724:38 UT (ionogram b) 2003 MLT, 3142 km, 65.5° Λ, $f_N/f_H = 0.26$ on ionogram a and 0.13 on ionogram b.

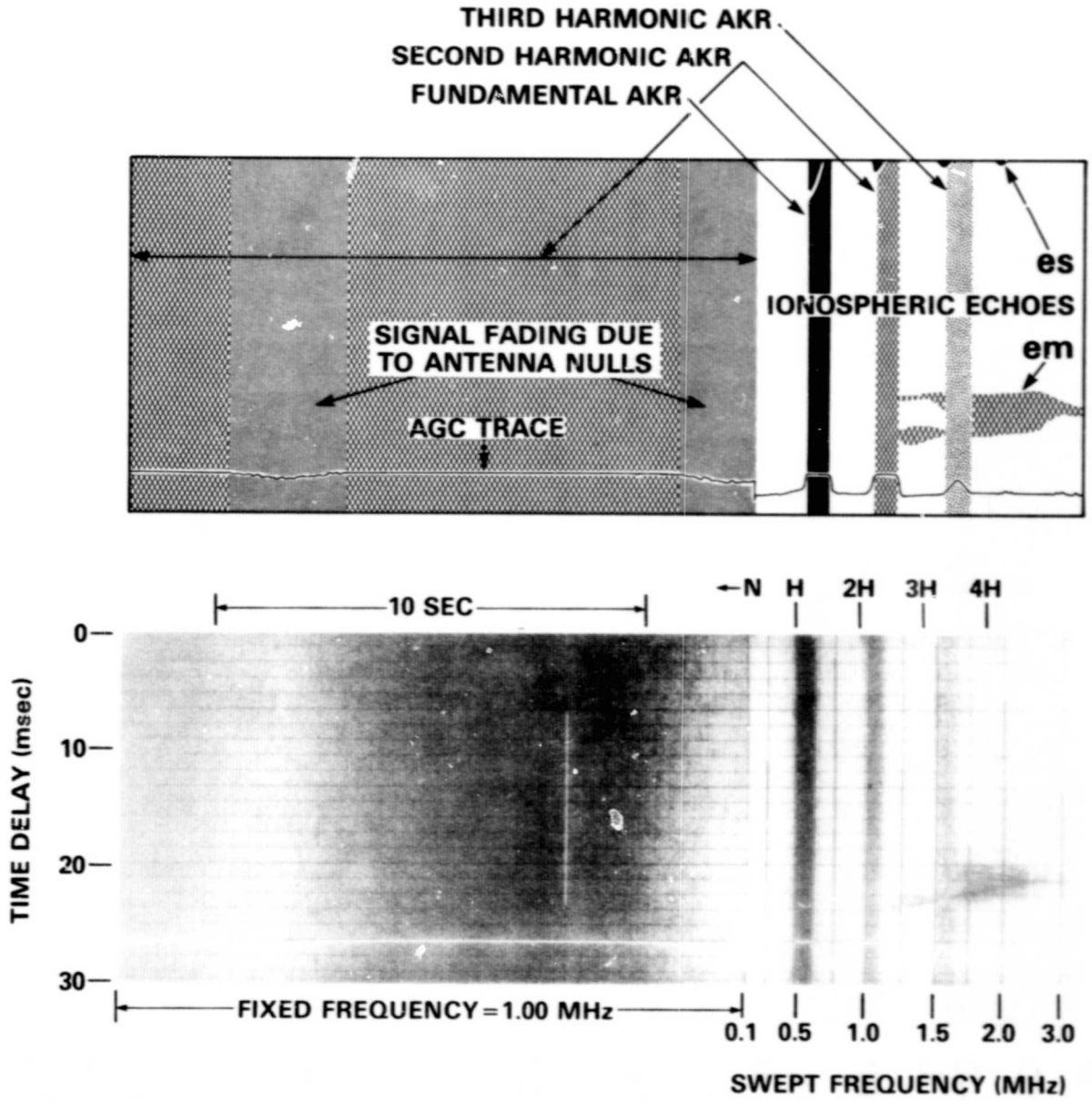

Figure 1

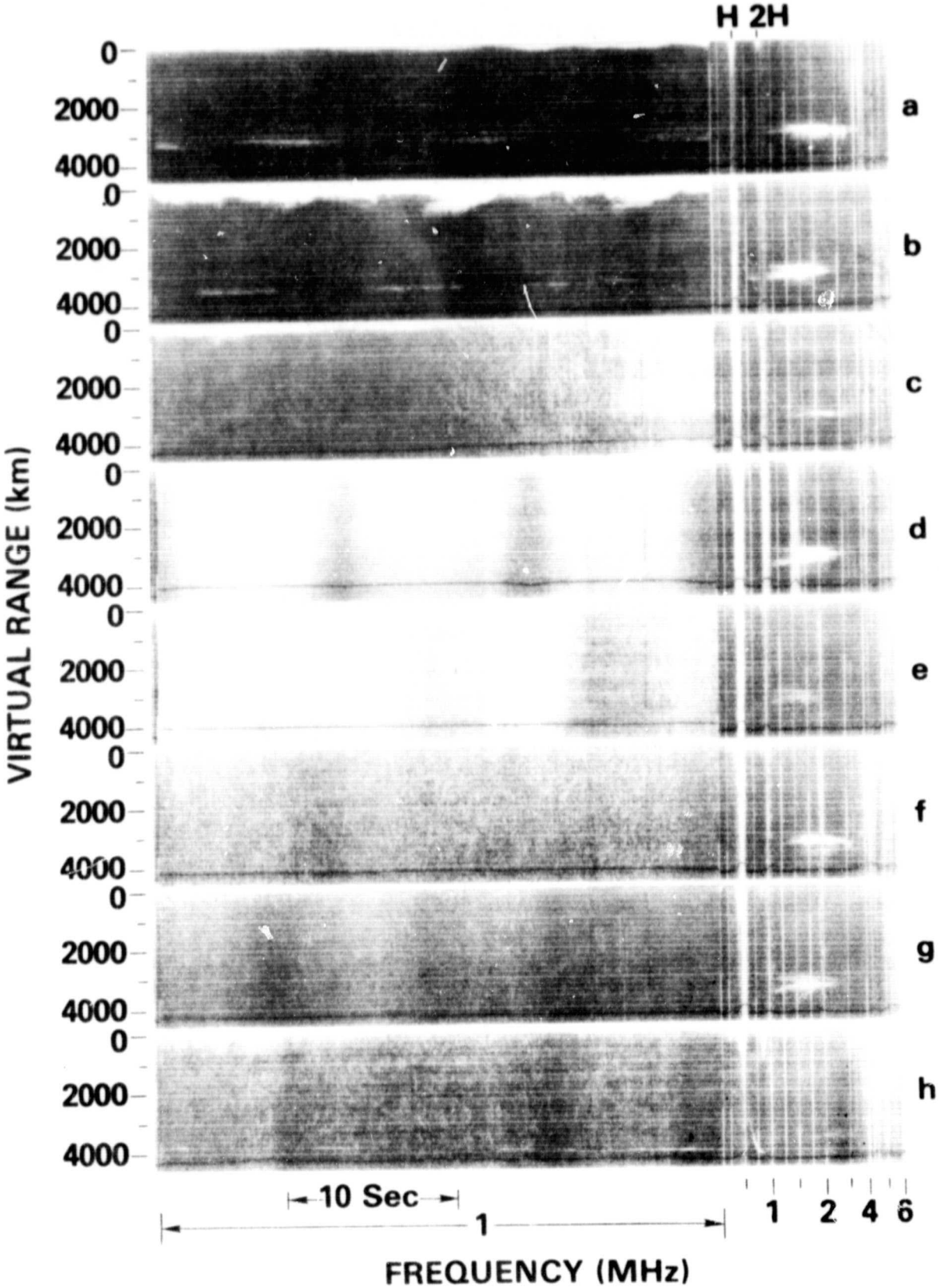

Figure 2

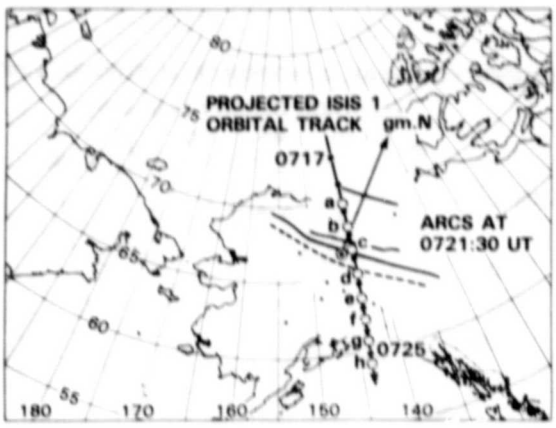

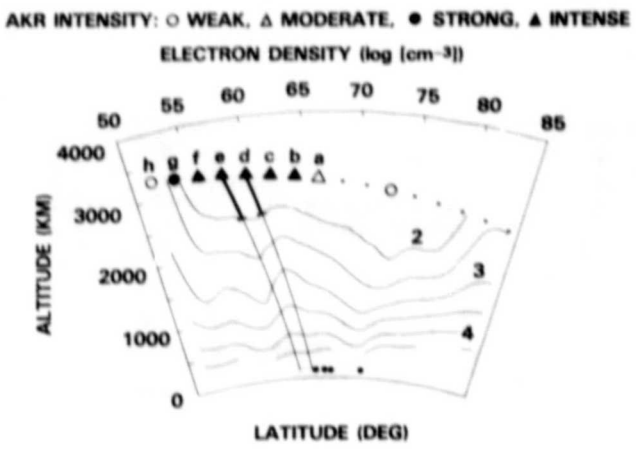

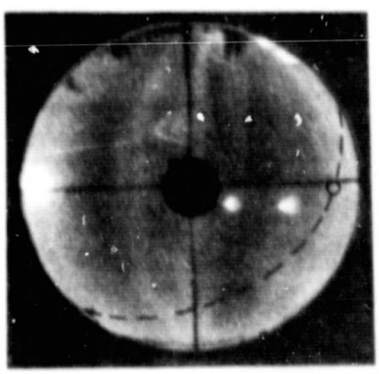

0720:00 UT

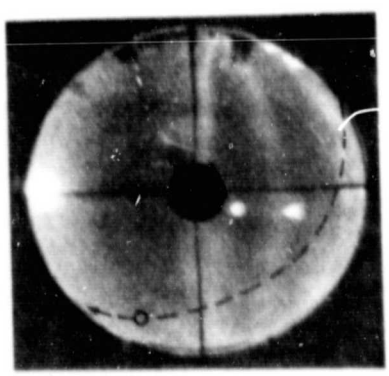

0721:30 UT

Figure 3

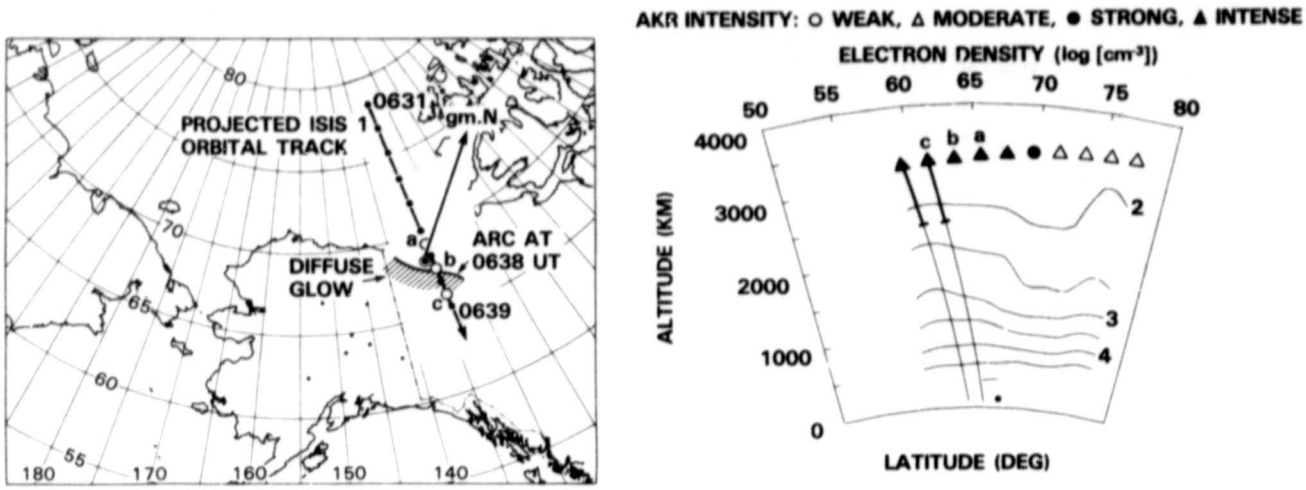

Figure 4

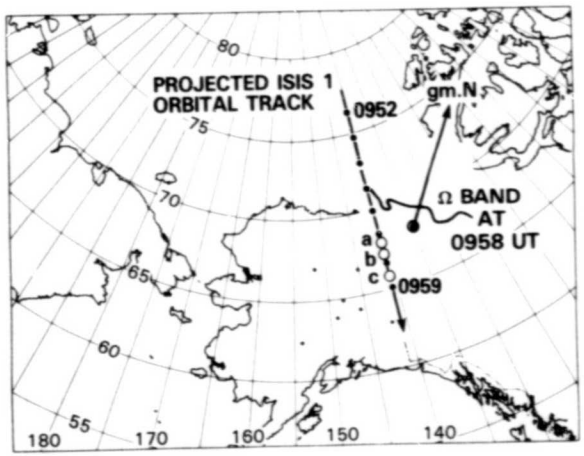

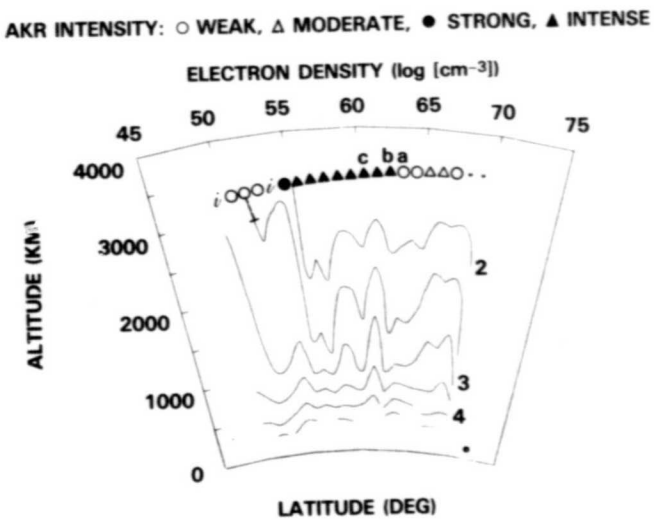

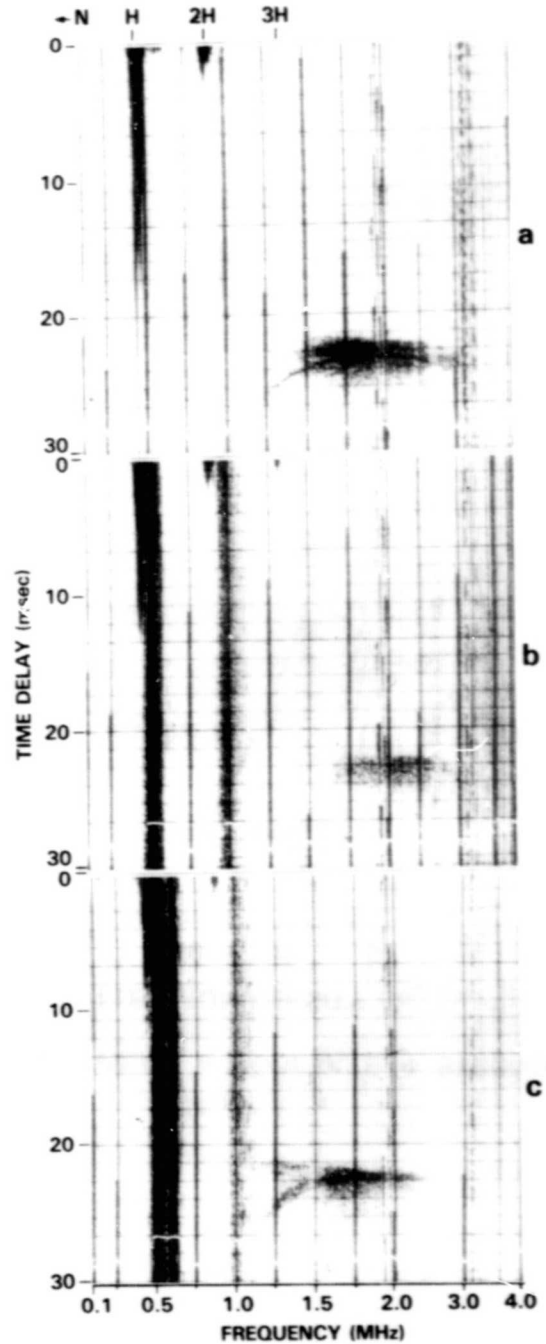

Figure 5

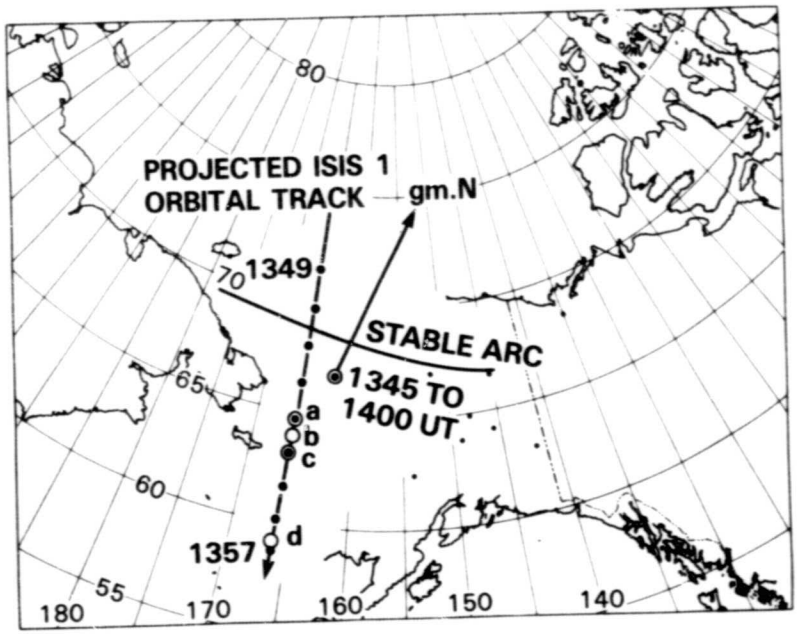

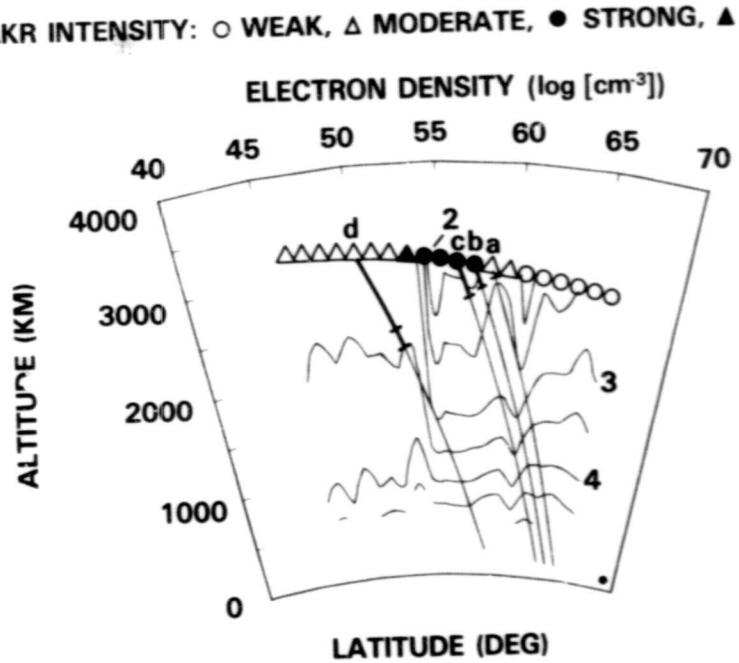

Figure 6

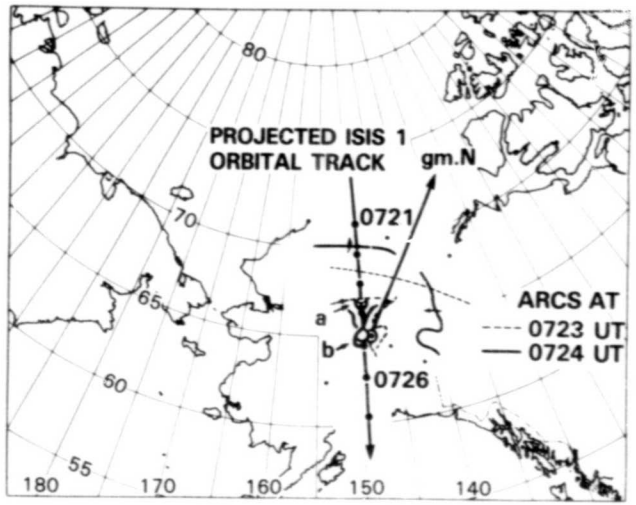

AKR INTENSITY: ○ WEAK, △ MODERATE, ● STRONG, ▲ INTENSE

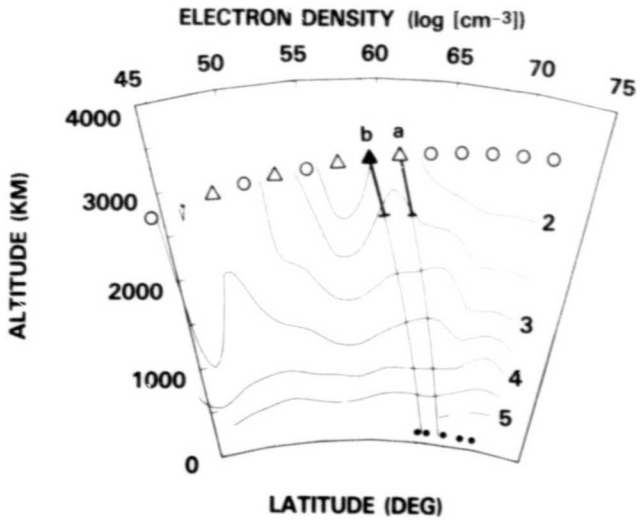

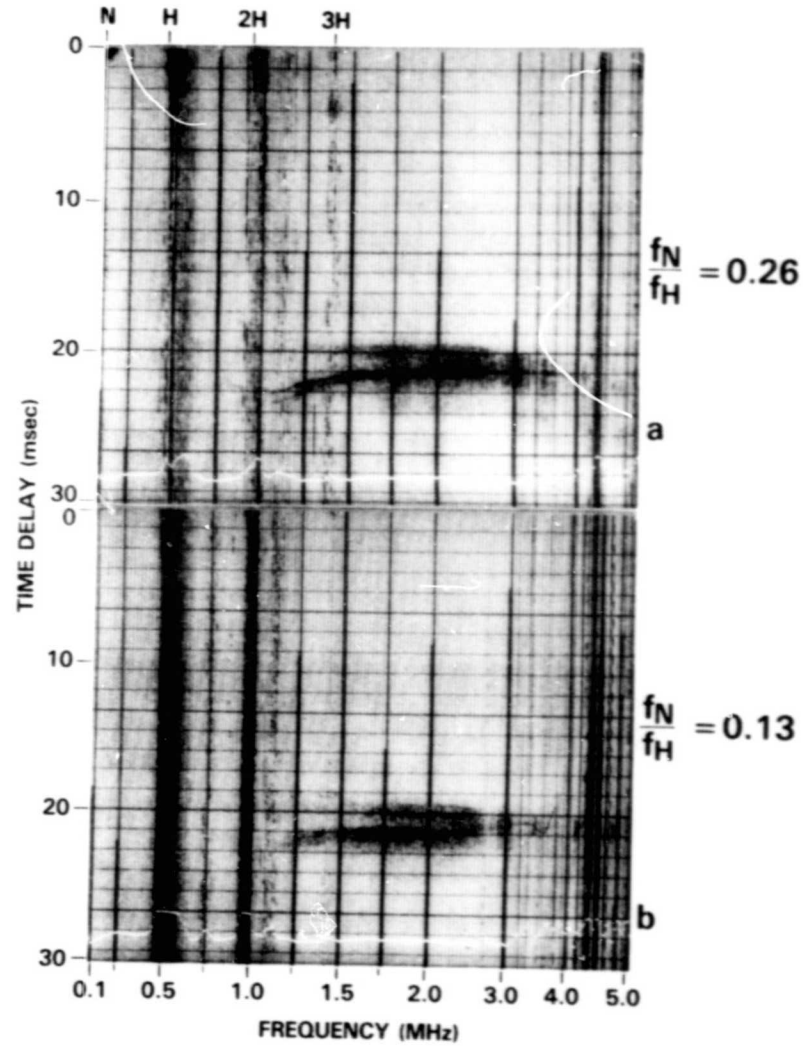

Figure 7